Weiyang Tong
Multidisciplinary Design
and Optimization Laboratory,
Department of Mechanical
and Aerospace Engineering,
Syracuse University,
Syracuse, NY 13244
e-mail: wtong@syr.edu

Souma Chowdhury
Mem. ASME
Department of Aerospace Engineering,
Center for Advanced Vehicular Systems,
Mississippi State University,
Starkville, MS 39759
e-mail: chowdhury@bagley.msstate.edu

Ali Mehmani
Multidisciplinary Design
and Optimization Laboratory,
Department of Mechanical
and Aerospace Engineering,
Syracuse University,
Syracuse, NY 13244
e-mail: amehmani@syr.edu

Achille Messac[1]
Professor
Fellow ASME
Department of Aerospace Engineering,
Mississippi State University,
Mississippi State, MS 39762
e-mail: messac@ae.msstate.edu

Jie Zhang
Mem. ASME
Transmission and Grid Integration Group,
National Renewable Energy Laboratory,
Golden, CO 80401
e-mail: jie.zhang@nrel.gov

Sensitivity of Wind Farm Output to Wind Conditions, Land Configuration, and Installed Capacity, Under Different Wake Models

In conventional wind farm design and optimization, analytical wake models are generally used to estimate the wake-induced power losses. Different wake models often yield significantly dissimilar estimates of wake velocity deficit and wake width. In this context, the wake behavior, as well as the subsequent wind farm power generation, can be expressed as functions of a series of key factors. A quantitative understanding of the relative impact of each of these key factors, particularly under the application of different wake models, is paramount to reliable quantification of wind farm power generation. Such an understanding is however not readily evident in the current state of the art in wind farm design. To fill this important gap, this paper develops a comprehensive sensitivity analysis (SA) of wind farm performance with respect to the key natural and design factors. Specifically, the sensitivities of the estimated wind farm power generation and maximum farm output potential are investigated with respect to the following key factors: (i) incoming wind speed, (ii) ambient turbulence, (iii) land area per MW installed, (iv) land aspect ratio, and (v) nameplate capacity. The extended Fourier amplitude sensitivity test (e-FAST), which helpfully provides a measure of both first-order and total-order sensitivity indices, is used for this purpose. The impact of using four different analytical wake models (i.e., Jensen, Frandsen, Larsen, and Ishihara models) on the wind farm SA is also explored. By applying this new SA framework, it was observed that, when the incoming wind speed is below the turbine rated speed, the impact of incoming wind speed on the wind farm power generation is dominant, irrespective of the choice of wake models. Interestingly, for array-like wind farms, the relative importance of each input parameter was found to vary significantly with the choice of wake models, i.e., appreciable differences in the sensitivity indices (of up to 70%) were observed across the different wake models. In contrast, for optimized wind farm layouts, the choice of wake models was observed to have marginal impact on the sensitivity indices. [DOI: 10.1115/1.4029892]

Keywords: Fourier amplitude sensitivity testing, mixed-discrete particle swarm optimization, sensitivity analysis, unrestricted wind farm layout optimization, wake model

1 Introduction

The energy from wind is generally harvested through wind farms, which can consist of hundreds of turbines. The primary loss of energy in a wind farm is attributed to the wake effects, which cause velocity deficits downstream of a turbine [1]. In practice, *wind farm layout optimization* (WFLO) can be applied to plan the micrositing of turbines, generally with the objective to minimize the wake-induced power losses [2]. Wake models are widely used to determine the wake-induced power losses. The effectiveness of estimating the wind farm power generation therefore relies on the accuracy and the reliability of the wake model used. Subsequently, factors regulating the wake behavior (wake growth and velocity deficit) also affect the power generation of a wind farm. In this context, it is important to understand how different natural and design factors impact the energy production and the economics of a wind farm and how these impacts vary with the choice of wake models.

In this paper, numerical experiments and SA are performed to investigate the relative impact of the following key factors on the wind farm power output: (i) incoming wind speed, (ii) ambient turbulence, (iii) land configuration (land area per MW installed and land aspect ratio), and (iv) nameplate capacity. Wind farms with both arraylike and optimal layouts are investigated to understand and explore their distinct sensitivity characteristics (with respect to these key factors). Single wake tests, individual factor wind farm analysis, and SA (all factors considered together) are all performed through the implementation of different wake models in the unrestricted WFLO (UWFLO) framework [3]. The SA strategy can also be applied in (and help further explore) other advanced WFLO frameworks recently reported in the literature [4–7]. Although each wake model primarily estimates the wake growth and the wake velocity deficits, this estimation could vary significantly—thereby demanding a better understanding (than currently available) of how the wake model itself synthetically regulates the sensitivity of wind farm performance to the different influencing factors. Four analytical wake models are taken into account for this purpose, namely, the Jensen model [8,9], the Frandsen model [10], the Larsen model [11,12], and the Ishihara model [13].

[1]Corresponding author.

Contributed by the Design Automation Committee of ASME for publication in the Journal of Mechanical Design. Manuscript received June 11, 2014; final manuscript received February 12, 2015; published online April 15, 2015. Assoc. Editor: Harrison M. Kim.

1.1 The Role of SA in Wind Energy.

SA is the "study of how the variation in the output of a model can be apportioned, qualitatively or quantitatively, to different sources of variation, and of how the given model depends upon the information fed into it" [14,15]. The findings of SA are expected to provide an important understanding to diverse researchers involved in the area of wind energy; it is particularly important to researchers from the engineering design community, who are involved in the wind energy optimization research at the wind turbine level, the wind farm level, as well as the wind energy market level. For example, an analytical wake model generally accounts for the downstream distance from the upstream turbine, the rotor diameter, the hub height, the incoming wind speed, and the ambient turbulence (as shown in Fig. 1). SA can help determine the most influential parameter (s) in this context to promote informed application and even further advancement of such wake models.

A significant amount of research has been done in the general area of SA of different aspects of wind farm dynamics. The modeling of wind energy production includes various correlated factors. SA is applied to determine the relative importance of the input parameters and identify the uncertainties existing in the energy production estimation process, thus helping improve the accuracy of the energy production estimation. Lackner et al. [16] proposed an approach to analyze the uncertainties that arise from assessing the wind resource, wind turbine power output and energy losses, and the overall energy production when using a Weibull distribution of wind speed. Rocklin and Constantinescu [17] applied a numerical weather prediction model to estimate the adjoint sensitivity of wind power generation and that of the cost of energy to wind speed. Kubik et al. [18] analyzed the sensitivity of the power generation of a wind turbine to wind shear coefficient and surface roughness. Capps et al. [19] evaluated the sensitivity of energy production of the Southern California wind farm to a series of key turbine design factors, including hub height, rated power, turbine rotor diameter, and turbine characteristic incremental cost.

SA has also been widely applied in the investigation of factors affecting wind energy economics. Fuglsang and Thomsen [20] investigated the sensitivity of the cost of energy of a large offshore wind farm to the turbine design variables, including hub height, rotor diameter, rotor speed, and rated power. Haughton et al. [21] performed a risk analysis to illustrate which factors impact the economic considerations in a wind energy project. Dykes et al. [22] used a directional impact graph to show the sensitivity of the overall performance and the cost of an offshore wind farm to the key turbine features, including rotor diameter, hub height, power rating, and the maximum tip speed. Dinwoodie et al. [23] applied SA method to analyze the uncertainty arising from the operation & maintenance (O&M) cost for offshore wind farms.

In addition, Martines et al. [24] preformed SA to show the sensitivity of the life cycle assessment of a multi-MW turbine to environmental factors. Gu et al. [25] used the sensitivity index to represent the impact of transmission congestion on wind generation curtailment. Zack et al. [26] performed the ensemble SA of the wind speed forecast with respect to changes in the prior values of atmospheric state variables. Osborn et al. [27] analyzed the sensitivity of wind farm factors in National Energy Modeling System to a series of assumptions used for modeling economic and physical conditions that affect wind resource assessment. Methodical exploration of the impact of wind farm-scale factors (on power output), e.g., land configuration and nameplate capacity, is however rare in the literature.

1.2 The Role of Wake Effects in Wind Farm Power Estimation. As wind flows across a turbine, the wind speed reduces and the turbulence intensity increases. Thus, a wake is formed behind the turbine, which affects the performance of downstream turbines. The wake not only progresses along the streamwise direction but also expands laterally. As a result, downstream turbines that are not coaxially downstream can be also affected by upstream turbine wakes. Collectively, this is called *the wake effects*. There are two major impacts of the wake effects on the entire wind farm: (i) it causes a deficiency in the overall energy output due to the velocity deficit in the wakes, and (ii) it causes a reduction of the turbine lifetime due to the additional turbulence induced structural loading. Factors affecting the wake behavior can be classified into two categories: natural factors and design factors.

Natural factors are primarily the variation in wind conditions (including wind speed, wind shear, and ambient turbulence) at the concerned farm site. These factors cannot be controlled through design or optimization. Design factors, on the other hand, are generally regulated by design decisions such as turbine locations, turbine features (e.g., turbine rotor diameter and hub height), land configuration, and number of turbines. These factors regulating the behavior of turbine wakes in turn affect the wind farm power generation. Therefore, the reliability of wind farm power estimation relies on the accuracy of the wake model used and on the assumptions associated with the natural and design factors.

The complex relationship between these factors and wind farm performance raises important questions in the context of wind farm analysis and optimization, as summarized below:

(1) What is the relative importance of each natural and design factor in the context of power output potential of a wind farm?
(2) Which of these factors can be neglected and/or assumed to be practically fixed in the process of wind farm optimization?
(3) How does the impact of these factors on the wind farm power output vary under the use of different wake models?

A comprehensive and coherent exploration of these questions is missing from the WFLO literature. An extensive SA study of the wind farm power output is hence performed in this paper, seeking to address the above questions. This study comprises two parts. In the first part, we conduct single wake test and a numerical experiment to show how the wind farm power estimation is influenced by the choice of wake models. This analysis provides interesting observations regarding how the impact of critical farm-scale factors (e.g., incoming wind speed or interturbine spacing) vary significantly with the choice of wake models. In the second part, the sensitivity of the power output capacity of both array-like wind farms and wind farms with optimized layouts are analyzed, under the implementation of different wake models. In this case, every optimal wind farm layout is determined by optimizing the locations of N turbines for a given incoming wind speed; here, the objective is to maximize the capacity factor (CF) of the wind farm under given allowed land configuration and minimum allowed inter-turbine spacing. The analyses led to unique findings

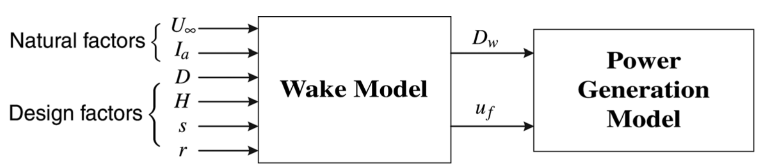

U_∞: Incoming wind speed | D: Turbine rotor diameter | s: Streamwise distance from the hub | D_w: Wake width
I_a: Ambient turbulence | H: Turbine hub height | r: Radial distance from the hub (perpendicular to s) | u_f: Velocity deficit (in the wake)

Fig. 1 General inputs and outputs of an analytical wake model

regarding how the sensitivity of the performances of an array-like layout and an optimum layout are different from each other, with respect to certain factors—indicating how optimization enhances or reduces the relative sensitivity indices.

In addition, factors related to turbine control play important roles in wind farm power generation and structural loading on the turbine [28–30]. For example, the wind turbine control system maintains a stable turbine power output to protect the system from hazardous loads and make the turbine rotor oriented perpendicularly to the incoming wind direction [31]. However, a majority of the research on the control of turbines (and its impact) generally focuses on the operation of single turbines [32]. Therefore, turbine control parameters are not considered in this paper.

The remainder of this paper is structured as described below: Section 2 presents the overview of the power generation model used in this paper. Section 3 describes the single wake test and the numerical experiment formulated to explore how the wind farm power generation is influenced by the choice of wake models. Section 4 performs the SA of the power output of both array-like wind farms and wind farms with optimized layouts, under the use of different wake models.

2 Wind Farm Power Estimation Using Analytical Wake Models

2.1 Power Generation Model. The power generation model used in this paper is adopted from the UWFLO framework [3], which is an advanced framework that allows optimal siting and selection of turbines subject to wind resource uncertainties. This power generation model quantifies the wind farm power output as a function of the turbine features, the location of turbines, and the incoming wind conditions [3]. A *generalized power curve* is used to evaluate the power output of each turbine. This *generalized power curve* is scaled back to represent the approximated power response of a particular commercial turbine, using the corresponding manufacturer specifications. For Turbine-i, the power generation, P_i, can be evaluated using the following equation:

$$\frac{P_i}{P_r} = \begin{cases} P_n\left(\dfrac{U_i - U_{\text{in}}}{U_r - U_{\text{in}}}\right), & \text{if} \quad U_{\text{in}} < U_i < U_r \\ 1, & \text{if} \quad U_r < U_i < U_{\text{out}} \\ 0, & \text{if} \quad U_{\text{out}} < U_i \quad \text{or} \quad U_i < U_{\text{in}} \end{cases} \tag{1}$$

where U_i is the velocity immediately in front of Turbine-i. Estimation of U_i accounts for wake merging scenarios and the possibility of partial wake–rotor overlap. U_{in}, U_{out}, and U_r are, respectively, the turbine cut-in, cut-out, and rated speeds, reported by the turbine manufacturer. The function P_n represents a polynomial fit for the *generalized power curve*, generated using the power curve data reported for the “GE 1.5 MW xle” turbine [33].

The UWFLO wind farm power generation model also allows for a variable induction factor. According to the 1D flow assumption [34], the induction factor a and the power coefficient, C_P, can be related by

$$C_P = 4a(1-a)^2 \tag{2}$$

where the power coefficient itself can be expressed as a function of incoming wind speed and turbine characteristics, as given by

$$C_P = \frac{P_i}{P_0} = \frac{P_i}{\frac{1}{8}\rho\pi D_i^2 U_\infty^3} \tag{3}$$

In Eq. (3), P_0 represents the power available from the wind, and U_∞ is the incoming wind speed at the hub height.

Subsequent solution of the nonlinear equation, Eq. (2), gives the induction factor for each turbine based on the estimated approaching wind conditions. Thereafter, the overall power output of a N-turbine wind farm, P_{farm}, can then be given by

$$P_{\text{farm}} = \sum_{i=1}^{N} P_i \tag{4}$$

It is important to note that the wake effects are integrated in this model, particularly in the process of determining the effective wind speed immediately in front of any turbine (U_i). Based on the predicted wake growth, the location of turbines, and the turbine features, an influence matrix is created to determine whether a turbine is influenced by the wake of other upstream turbines for a given wind direction. As a result, the velocity immediately in front of each turbine is dynamically evaluated using a wake model, and in the same order in which the turbines encounter the wind coming from a particular direction. The Katic model [9] is used here to account for the wake merging and partial wake–rotor overlap. If Turbine-i is in the influence of multiple wakes created by K upstream turbines, the corresponding velocity deficit, v_i, is given by

$$v_i = \sqrt{\sum_{k=1}^{K} \frac{A_{ki}}{A_i}\left(u_f^{ki}\right)^2} \tag{5}$$

where u_f^{ki} represents the velocity deficit in the wake (created by Turbine-k) at the location of Turbine-i, and A_{ki} is the effective influence area of the wake (created by Turbine-k) on Turbine-i. If Turbine-i is completely in the wake of Turbine-k, $A_{ki} = A_i$; otherwise, A_{ki} denotes the overlapping area between the wake of Turbine-k and Turbine-i, estimated by standard geometrical intersection formula.

2.2 Analytical Wake Models. The wake models studied in this paper are analytical wake models, and each model was originally derived for specific scenarios (empirical equations, farm site-based experiments, etc.). However, in the context of WFLO problems, the computational efficiency of a particular analytical wake model is an important consideration driving the choice of model. Table 1 shows a comparison of the computation time of each wake model for a two turbines scenario [35–39]. It is readily evident that analytical wake models are the most suitable for WFLO problems. Hence, analytical wake models are preferred in WFLO (e.g., Jensen model [4,6,7] and Frandsen [3,5]).

Several studies/projects emphasize the validation of wake models through comparisons with test cases, to understand the limitations and define clear guidelines regarding how each of the wake models should be applied [40–43]. For example, Jensen model has been proven to be reliable for long-term power predictions in small to medium size wind farms [8,9]. Refs. [41,44,45] have also shown that the accuracy of a wake model decreases when wind direction sectors are smaller than 10 deg. Additionally, model validation also highly depends on the quantity and quality of the wind data acquired from real farm sites (e.g., anemometer data may be inadequate) [43].

This paper focuses on investigating the impact of analytical wake models on the wind farm power estimation and how different optimal layout patterns result from using different wake

Table 1 Comparison of computation time of wake simulation for two turbines in line [39]

Wake model	Computation time	Model type
Jensen model [8,9]	5 s	Analytical
Actuator disk model [35]	25 s	Actuator disk
Dynamic Wake Meandering model [36]	8 min	Analytical + actuator disk
SOWFA [37,38]	30 hr	3D CFD

Table 2 Analytical wake model inputs

Input to wake model	Jensen	Frandsen	Larsen	Ishihara
Incoming wind speed	✓	✓	✓	✓
Streamwise distance from hub	✓	✓	✓	✓
Radial distance from hub			✓	✓
Rotor diameter	✓	✓	✓	✓
Hub height			✓	
Turbulence intensity			✓	✓

models in the WFLO process. Four analytical wake models are implemented in this paper and compared for the purpose of quantifying wake-induced power losses, both in a given layout and for layout optimization. Table 2 lists the general input parameters considered in each wake model. Further mathematical description of the wake models can be found in Refs. [8–13].

3 Impact of Different Analytical Wake Models on Wind Farm Power Estimation

This section investigates the impact of using different analytical wake models (I) on the wake behavior downstream of turbines, and (II) on the relationship of wind farm power generation to land area and nameplate capacity. Careful numerical experiments are designed to illustrate the variation in wake behavior and the variation of the wind farm power generation with unit land area and incoming wind speed.

3.1 Numerical Settings. We assume a rectangular wind farm with 16 GE 1.5 MW xle turbines arranged in a 4×4 array-like layout, as shown in Fig. 2. The power characteristics of GE 1.5 MW xle turbine is shown in Fig. 3, and Table 3 lists the turbine specifications. The range of incoming wind speed is varied between the turbine cut-in speed and cut-out speed. The land area per MW installed, A_{MW}, is used to represent the unit land area. The range of A_{MW} is specified as

$$10\frac{D^2}{P_r} < A_{\mathrm{MW}} < 30\frac{D^2}{P_r} \tag{6}$$

where P_r is the turbine rated power in MW. This range of land area per MW installed spans from a very stringent (small) land footprint to practically average land footprint which is a range of interest for future wind farms, considering that generous land footprint has undesirable impact on surroundings. This range was used for a land area-energy production analysis by Chowdhury et al. [46] and was derived from the land area of currently operational U.S. wind farms, reported by Ref. [47]. For a GE 1.5 MW xle turbine, the rated power is 1.5 MW. Since identical turbines are considered, the numerical range of the land area per turbine (LAT), A_T, is given by

$$70,000\,\mathrm{m}^2 \le A_T \le 200,000\,\mathrm{m}^2 \tag{7}$$

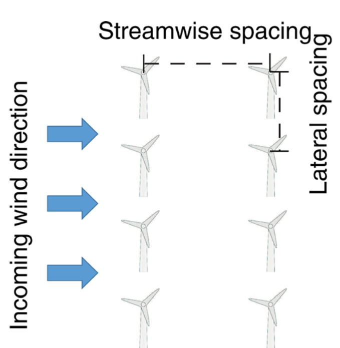

Fig. 2 An arraylike farm layout with 16 GE 1.5 MW xle turbines

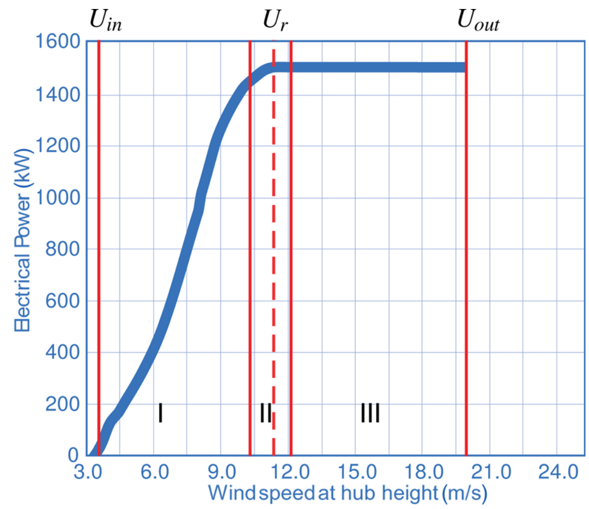

Fig. 3 Power curve of GE 1.5 MW xle turbine [33]

We assume that all turbines are uniformly arranged, and the land aspect ratio is fixed at 7/3. Hence, the effective inter-turbine spacing is regulated by the LAT. We also assume a unidirectional wind condition, a constant ambient turbulence intensity over the farm site, and a uniform incoming velocity profile over the rotor area. The ratio of the longitudinal (or streamwise) spacing and the lateral spacing between turbines is also maintained at 7/3.

The wind farm CF is used as a measure of wind farm production performance. For a wind farm with identical turbines, the wind farm CF is defined as the ratio of the actual power generation of the wind farm to the nameplate capacity of the wind farm, which is given by

$$\mathrm{CF} = \frac{P_{\mathrm{farm}}}{P_{\mathrm{NC}}} \tag{8}$$

where P_{NC} is the nameplate capacity of the concerned wind farm. The parameter P_{farm} is the actual power generated by the wind farm, as estimated by the UWFLO power generation model; this model allows the use of any of the four wake models. The results from the two different numerical experiments, i.e., the single wake test and the wind farm power analysis, are discussed in Sections 3.2 and 3.3, respectively.

3.2 Single Wake Analysis. The single wake test provides important insights into the distinguishing characteristics of the wake behavior, simulated by different wake models. The GE 1.5 MW xle turbine is used in this test (Table 3). Additionally, since far wake scenarios are mostly considered (i.e., in practice, turbines are unlikely to be located within each other's near wakes), the simulation of wake behaviors starts at two rotor diameters downstream from the turbine.

Figures 4(*a*) and 4(*b*) present the wake expansions and the wake speeds behind the GE 1.5 MW xle turbine, as estimated by the four analytical wake models. It is observed that, along the entire flow field, the Frandsen model predicts the highest wake speed, and the Larsen model predicts the largest wake diameter. It

Table 3 Specifications of GE 1.5 MW xle turbine [33]

Specifications	Value
Rated power (P_r)	1.5 MW
Turbine rotor diameter (D)	82.5 m
Hub height (H)	80 m
Cut-in speed (U_{in})	$3.5\,\mathrm{m}\cdot\mathrm{s}^{-1}$
Cut-out speed (U_{out})	$20\,\mathrm{m}\cdot\mathrm{s}^{-1}$
Rated speed (U_r)	$11.5\,\mathrm{m}\cdot\mathrm{s}^{-1}$

is also observed that the Ishihara model predicts the lowest wake speed; however, it also yields the highest rate of wake recovery. This phenomenon can be attributed to the greater mixing of the turbine wake with the upper layers of the atmospheric boundary layer, which is facilitated by the turbine-induced turbulence, specifically accounted for in the Ishihara model. It is important to note (from Fig. 4(*a*)) that, in the practically popular range of farm inter-turbine spacing (of 7D–10D), the difference in the wake speeds estimated by the four wake models is approximately 15–20%.

3.3 Wind Farm Power Generation Analysis

3.3.1 Power Variation With the LAT. Figures 5(*a*)–5(*d*) show the variation of the wind farm CF with the LAT, estimated at different values of incoming wind speed. Among the four analytical wake models, the Frandsen model predicts the largest CF, while the Ishihara wake model predicts the smallest; this trend holds true over the entire range of LAT studied and the different incoming wind speeds considered. **Three scenarios** are observed based on the flow patterns inside the wind farm.

Scenario one: When the incoming wind speed is close to the turbine cut-in speed, the downstream turbines most likely do not start generating power, since the wake speeds encountered by these turbines are lower than the turbine cut-in speed. As shown in Fig. 5(*a*), when the incoming wind speed is $4\,\mathrm{m \cdot s^{-1}}$, the CF predicted using the Frandsen model or the Jensen model shows some variation with the LAT. This is attributed to their relatively high predicted wake speeds, as shown in Fig. 4(*a*). For the cases using Larsen model and Ishihara model, due to their relatively lower wake speed estimates, the predicted CFs show almost no variation with the LAT (within the specified ranges).

Scenario two: The wake speed in front of the downstream turbines is expected to be higher than the turbine cut-in speed in this case. The flow pattern inside the wind farm now becomes more complex owing to the combined influence from the wake effects and the inter-turbine spacing regulated by the LAT. As shown in Fig. 5(*b*), the CFs predicted using all four wake models are varying with the LAT. It is observed that although the CF improves as the LAT increases, as the incoming wind speed is approaching the turbine rated speed, the variation of the predicted CF with the LAT becomes less prominent.

Scenario three: This scenario is observed when turbines in the first row reach the rated power. As shown in Fig. 5(*c*), the CF predicted using the Frandsen model, the Jensen model, or the Larsen model shows marginal to no variation with LAT (the predicted value is slightly below 100% due to the wake effects). However, this is not the case with the Ishihara model due to its relatively lower wake speeds estimation. As the incoming wind speed continues to increase, the velocity in front of all the downstream turbines also exceeds the turbine rated speed. Therefore, all downstream turbines are then able to reach the rated power, leading to a 100% CF. In Fig. 5(*d*), the CF predicted using the Jensen model or the Frandsen model has reached 100%. If the incoming wind speed continued to increase beyond $12\,\mathrm{m \cdot s^{-1}}$, the Larsen model and the Ishihara model will also lead to 100% CF estimates.

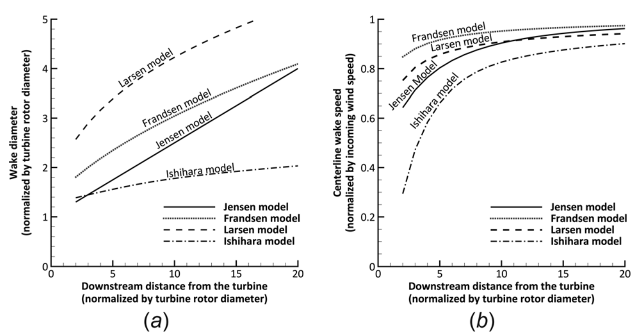

Fig. 4 Single wake test. (*a*) Wake diameter behind a GE 1.5 MW xle turbine and (*b*) wake speed behind a GE 1.5 MW xle turbine.

3.3.2 Power Variation With the Incoming Wind Speed. The variations of the CF with incoming wind speed are investigated at selected values of LAT, as shown in Figs. 6(*a*)–6(*c*). The "normalized power curve" (indicted by a light gray curve) represents the polynomial fit for the *generalized power curve* normalized with respect to the turbine rated power. Among the four analytical wake models, we observe that the Frandsen model predicts the highest CF, while the Ishihara wake model predicts the lowest CF. It is observed that, owing to the wake effects, all the predicted CF curves asymptotically approach the normalized power curve when the LAT increases. In addition, the difference between the CFs predicted using different wake models slightly decreases as the LAT increases.

4 SA of Wind Farm Power Output

In this section, we analyze the sensitivity of wind farm output to five key factors, which include (i) incoming wind speed (U_∞), (ii) ambient turbulence (I_a), (iii) land area per MW installed (A_{MW}), (iv) land aspect ratio (a_r), and (v) nameplate capacity (P_{NC}). Two numerical experiments are conducted to perform the SA using the GE 1.5 MW xle turbines (Table 3). Numerical experiment I examines the sensitivity of the power output of an array-like wind farm to the first four input parameters. The wind farm is assumed to have 16 turbines installed on a 4×4 array layout. In numerical experiment II, we investigate the sensitivity of the maximized wind farm output to all five input parameters. The maximized wind farm output is obtained by WFLO, which is performed using the mixed-discrete Particle Swarm Optimization algorithm (from the UWFLO framework) [3,48]. The assumptions made in the case of these two numerical experiments are summarized below:

(1) Wind shear effect is not considered in this paper; the incoming velocity is assumed to be uniform over the entire rotor area (rotor-averaged velocity);
(2) Identical turbines are considered;
(3) The wind farm has a rectangular shape; and

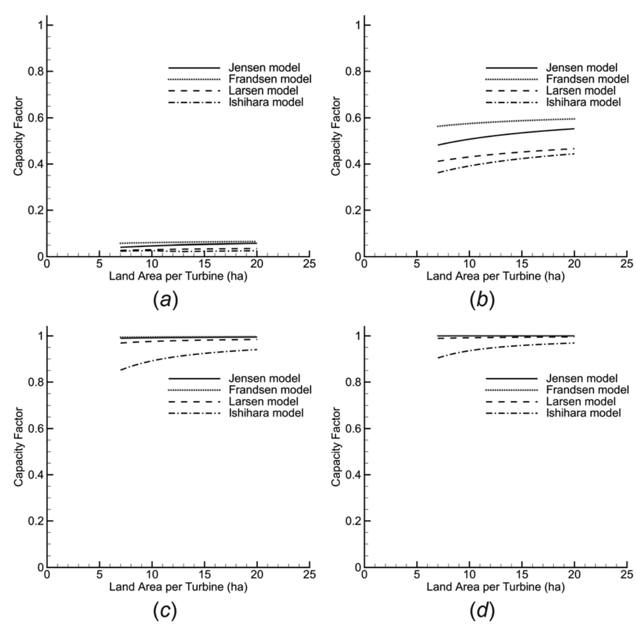

Fig. 5 Variation of the CF with the LAT. Incoming wind speed of (*a*) $4\,\mathrm{m \cdot s^{-1}}$ (slightly above the turbine cut-in speed), (*b*) $8\,\mathrm{m \cdot s^{-1}}$ (in between the turbine cut-in and rated speeds), (*c*) $11.5\,\mathrm{m \cdot s^{-1}}$ (at the turbine rated speed), and (*d*) $12\,\mathrm{m \cdot s^{-1}}$ (slightly above the turbine rated speed).

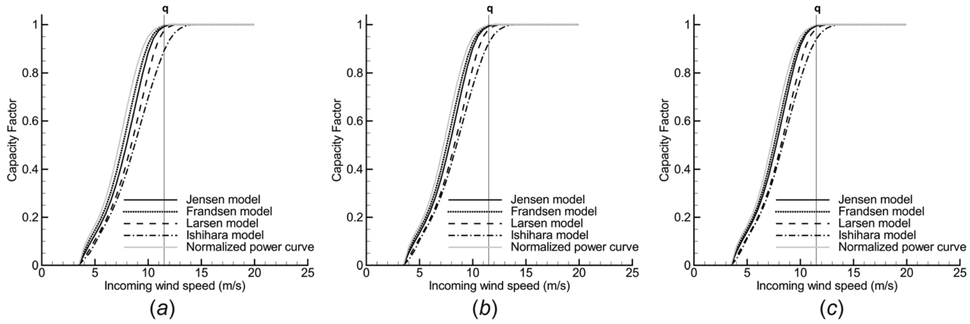

Fig. 6 Variation of the CF with the incoming wind speed. LAT of (a) 15 ha, (b) 20 ha, and (c) 25 ha.

(4) The ambient turbulence over the farm site is constant everywhere.

The e-FAST method is used to perform the SA. An overview of the e-FAST method is provided in Section 4.1.

4.1 Overview of the e-FAST. The e-FAST method developed by Saltelli and Bolado [49] is adopted in this paper, which is an advanced version of the original FAST method proposed by Ckuier et al. [50–53]. The primary advantage of e-FAST method is the ability to determine both the first-order and the total-order sensitivity indices. The first-order index, also known as the main effect, illustrates the variance of the model output due to each of the input parameters. To estimate the first-order index, the input parameters of a model are transformed into a frequency domain using Fourier transformation. Thus, a multidimensional model is reduced into a model with a single dimension. In the original FAST method [50], for a model with n input parameters, $X=\{x_1,x_2,\ldots,x_n\}$, the output of the model, Y, is expressed as $Y=f(x_1,x_2,\ldots,x_n)$.

A search function is defined to allow the input parameter to oscillate periodically in the input space, by assigning a characteristic frequency ω_i, expressed as

$$x_i = G_i(\sin\omega_i s), \quad i=1,2,\ldots,n \tag{9}$$

Here, G_i is a transform function, and $s\in(-\infty,+\infty)$ is a scalar.

By applying the properties of Fourier series, $E(Y)$ can be expressed as

$$Y=f(s)=A_0+\sum_{k=1}^{+\infty}[A_k\cos(ks)+B_k\sin(ks)] \tag{10}$$

where $f(s)=f(x_1(s),x_2(s),\ldots,x_n(s))$, and $i=1,2,\ldots,n$; A_0, A_k, and B_k are the Fourier coefficients, defined as

$$A_0=\frac{1}{2\pi}\int_{-\pi}^{\pi}f(s)ds,\text{ and}$$
$$A_k=\frac{1}{\pi}\int_{-\pi}^{\pi}f(s)\cos(ks)ds,\quad B_k=\frac{1}{\pi}\int_{-\pi}^{\pi}f(s)\sin(ks)ds \tag{11}$$

For practical problems, k must be limited to a reasonable value of the integer N, which indicates the sample size of the input data. The variance of the model output, s_Y^2, can therefore be approximated as

$$s_Y^2=E(Y^2)-[E(Y)]^2\approx\frac{1}{2\pi}\sum_{k=1}^{(N-1)/2}\left(A_k^2+B_k^2\right)$$
where
$$A_k=\frac{1}{\pi}\sum_{j=1}^{N}f(s_j)\cos(s_jk),\quad B_k=\frac{1}{\pi}\sum_{j=1}^{N}f(s_j)\sin(s_jk) \tag{12}$$

In the variance-based SA, the first-order sensitivity index of an input parameter, x_i, is defined as the conditional variance of the model output, $s^2_{E(Y/x_i)}$, with respect to the unconditional variance of the model output (s_Y^2). To measure this conditional variance, the expectation value of x_i, $E(Y/x_i)$, must be evaluated throughout the entire interval of x_i. In the FAST method, the conditional variance is approximated by summing up the spectrum values for the basic frequency ω_i and its higher harmonics, as shown below:

$$s^2_{E(Y/x_i)}\approx\frac{1}{2}\sum_{p=1}^{m}\left(A^2_{p\omega_i}+B^2_{p\omega_i}\right) \tag{13}$$

In Eq. (13), $p\in Z$ and $p\omega_i\le(N-1)/2$; and m indicates the order of higher harmonics that are considered [53].

Therefore, the first-order index can be formulated by combining Eqs. (13) and (12), which is expressed as

$$S_i=\frac{s^2_{E(Y/x_i)}}{s_Y^2} \tag{14}$$

The total-order sensitivity index includes the interactions between the input parameters of any order. The e-FAST method uniquely accounts for interactions by considering the complementary set of the conditional variance, corresponding to the ith input [14]. Here, we use "$\neq i$" to denote "all except i." Hence, the conditional variance, $s^2_{E(Y/x_{\neq i})}$, is expressed as

$$s^2_{E(Y/x_{\neq i})}=2\sum_{p=1}^{m}\left(A^2_{p\omega_{\neq i}}+B^2_{p\omega_{\neq i}}\right) \tag{15}$$

The total-order index is thus given by subtracting the variance due to all other input parameters from 1, that is

$$S_{Ti}=1-\frac{s^2_{E(Y/x_{\neq i})}}{s_Y^2} \tag{16}$$

4.2 Upper and Lower Bounds of Input Parameters. The process of SA of the wind farm output could become expensive even under the use of analytical wake models. It is therefore important to have a computationally efficient approach to implement the SA. As a result, the selection of the upper and lower bounds of different natural and design factors influencing the wind farm power estimation is an important step in itself. It requires significant prior understanding of the area of WFLO. In this paper, five input parameters are investigated, including two natural factors (incoming wind speed and ambient turbulence) and three design factors (land area per MW installed, land aspect ratio, and nameplate capacity). The ranges of all input parameters are specified with the objective to focus on the variation or range that is most likely to occur in practice.

The upper and lower bounds of incoming wind speed are set as the turbine cut-in speed $(3.5\,\mathrm{m\cdot s^{-1}})$ and cut-out speed

Table 4 Upper and lower bounds of natural factors

Natural factors	Case 1 (region I)		Case 2 (region II)		Case 3 (wind speed class IV)	
	Lower bound	Upper bound	Lower bound	Upper bound	Lower bound	Upper bound
Incoming wind speed ($\mathrm{m \cdot s^{-1}}$)	3.5	10.35	10.35	12.1	7.0	7.5
Ambient turbulence (%)	10	25	10	13	14	16

Table 5 Upper and lower bounds of design factors

Design factors	Lower bound	Upper bound
Land area per MW installed	10 ha/MW	50 ha/MW
Land aspect ratio	0.1	10
Nameplate capacity	15 MW	150 MW

($20\,\mathrm{m \cdot s^{-1}}$), respectively. Based on the nature of the turbine power curve, the incoming wind speed can be divided into three regions as shown in Fig. 3. In the first region where the incoming speed is below the turbine rated speed, the farm power output is highly sensitive to the incoming wind speed. The second region is a transient region, where the power output may be variably sensitive to the incoming wind speed depending on the deg of the wake-induced power losses. This is because the wake-induced losses can drive the incoming wind from Region II to Region I for the downstream rows of turbines. Hence, the incoming wind speed in this region is ranged from 10% below to 5% above the turbine rated speed. In the third region, the power output of the farm is weakly sensitive or not sensitive to the incoming wind speed variations. In this case, even after wake losses, the wind speed approaching the downstream turbines within the farm remain above the rated speed, unless the farm comprises a very large number of turbines (that would then lead to substantial cumulative wake losses). Therefore, SA is only performed in the first two regions (defined in Fig. 3), i.e., case 1 and case 2, respectively. Additionally, a new case (case 3) is defined to investigate the variation of incoming wind speed in the range representing wind speed Class IV (between $7\,\mathrm{m \cdot s^{-1}}$ and $7.5\,\mathrm{m \cdot s^{-1}}$). The purpose of case 3 is to better understand the impact of the four input parameters other than wind speed, as these impacts are otherwise grossly overshadowed by the influence of wind speed in case 1 and case 2.

The variation range of the ambient turbulence in this paper is specified from 0.1 to 0.25, which is determined based on the representative turbulence intensity given by IEC-61400-1 [54].

The land aspect ratio, a_r, is varied between 0.1 and 10. The range of land area per MW installed is set between 10 ha/MW and 50 ha/MW, based on the reported average unit land usage of U.S. commercial wind farms in 2009 (34.5 ± 22.4 ha/MW) [47]. The number of turbines is ranged from 10 to 100. Since identical turbines are considered, the nameplate capacity therefore varies between 15 MW and 150 MW. Owing to the computational constraints, the nameplate capacity is limited to 150 MW, which is the level of a midscale wind farm. The trends obtained are, however, expected to hold for wind farms with larger number of turbines.

Tables 4 and 5 list the detailed upper and lower bounds specified for the natural and design input parameters, respectively. It is important to note that the upper and lower bounds of the natural input parameters are specified differently for each case, whereas those for the design input parameters are fixed across all three cases.

4.3 Numerical Experiment I: SA of the Power Output of Wind Farms With Array-like Layouts. In this study, the sample size of each input parameter is set at 1000. Figure 7 presents the sensitivity of wind farm power output to the four input parameters. In this case, the incoming wind speed is between $3.5\,\mathrm{m \cdot s^{-1}}$ and $10.35\,\mathrm{m \cdot s^{-1}}$ (case 1). How the choice of wake models affect the sensitivity of the estimated power output to the input parameters is shown in Figs. 7(*a*)–7(*d*). It is observed that the impact of incoming wind speed on the wind farm power output is dominant, irrespective of the choice of wake models. Both the first-order and the total-order sensitivity indices of the incoming wind speed are close to 1.

Figures 8(*a*)–8(*d*) show the SA performed in case 2, where the variation of incoming wind speed is limited to a small range around the turbine rated speed (between $10.35\,\mathrm{m \cdot s^{-1}}$ and $12.1\,\mathrm{m \cdot s^{-1}}$). In case 2, it is observed that the relative impact of the input parameters varies appreciably with the choice of wake models. Under all the four wake models, the incoming wind speed still remains the decisive factor affecting the power output. On closer observation, the power output predicted using the Frandsen model (Figs. 8(*b*)) is found to be the most sensitive to the incoming wind speed, which can be attributed to the tendency of the Frandsen model to yield relatively high wake speeds (Fig. 4(*b*)).

In contrast, the land aspect ratio appears to be the most important input parameter when using the Ishihara model (Fig. 8(*d*)); this is an important observation considering that the role of land shape (or aspect ratio) in wind energy production has not been comprehensively investigated either in the turbulence/Atmospheric Boundary Layer (ABL) community or in the wind farm design community. It is also interesting to note that, irrespective of the choice of wake models, the land aspect ratio has a relatively stronger impact than the land area per MW installed. Overall, in case 2, it is observed that the total-order sensitivity index of each input parameter is substantially higher than the corresponding first-order index, when compared to the results obtained in case 1. This observation indicates that the influences of different factors on the farm are highly coupled, which is indirectly also representative of the high nonlinearity of the wind farm power output function. This in turn implies that, in planning wind farm layouts, one needs to carefully consider the interactions between the input factors, which have not always been the case in conventional wind farm design.

Case 3 considers the standard wind class IV as the defined range of incoming wind speed. This case is intended to illustrate the relative importance of the input parameters other than wind speed. The sensitivity results of case 3 are shown in Figs. 9(*a*)–9(*d*). It is observed that the relative importance of the input parameters varies significantly with the choice of wake models. When using the Frandsen model or the Larsen model (Figs. 9(*b*) and 9(*c*)), the wind farm power output is still mostly regulated by the incoming wind speed; while under Jensen model and Ishihara model (Figs. 9(*a*) and 9(*d*)), land aspect ratio is the most decisive input parameter that regulates the power output. When comparing these results with the single wake test, we can readily identify that the relative influence of incoming wind speed (in terms of wake model choice) on the wind farm power estimation follows the same order as that of the wake speeds estimated by the four different wake models.

4.4 Numerical Experiment II: SA on Maximized Farm Output With Optimal Layouts. In the second numerical experiment, the sensitivity of the maximized farm output is analyzed with respect to five input parameters, including nameplate capacity in addition to those considered in the numerical experiment I. The sample size of each input parameter is again set to 1000. Conditions under cases 1 and 2 (Table 4) are also explored in this numerical experiment.

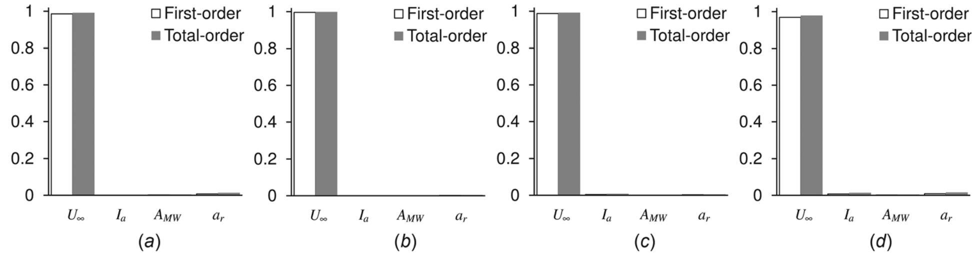

Fig. 7 SA of the power output of a wind farm with a 4 × 4 array layout (case 1). (*a*) Jensen model, (*b*) Frandsen model, (*c*) Larsen model, and (*d*) Ishihara model. U_∞: Incoming wind speed; I_a: ambient turbulence; A_{MW}: land area per MW installed; a_r: land aspect ratio.

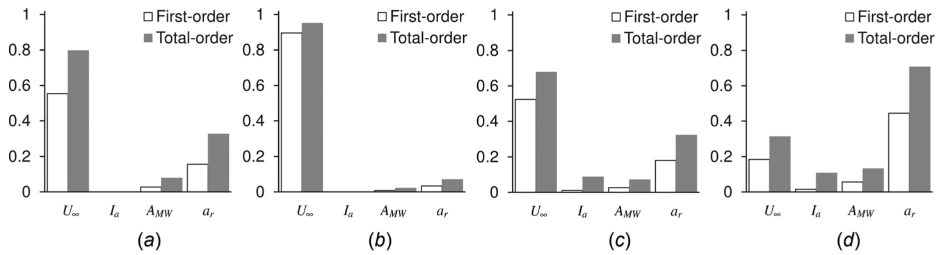

Fig. 8 SA of the power output of a wind farm with a 4 × 4 array layout (case 2). (*a*) Jensen model, (*b*) Frandsen model, (*c*) Larsen model, and (*d*) Ishihara model. U_∞: Incoming wind speed; I_a: ambient turbulence; A_{MW}: land area per MW installed; a_r: land aspect ratio.

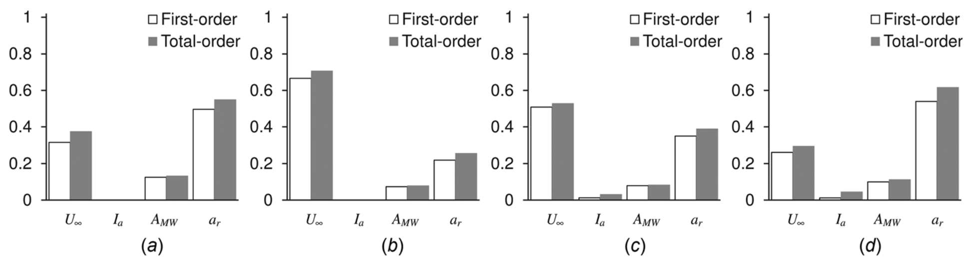

Fig. 9 SA of the power output of a wind farm with a 4 × 4 array layout (case 3). (*a*) Jensen model, (*b*) Frandsen model, (*c*) Larsen model, and (*d*) Ishihara model. U_∞: Incoming wind speed; I_a: ambient turbulence; A_{MW}: land area per MW installed; a_r: land aspect ratio.

The WFLO takes each combination of the sample input parameters as a given condition. Since identical turbines are considered, the number of turbines to be installed is readily determined based on the given sample value of the nameplate capacity. However, as the number of turbines for each WFLO may be different, the wind farm capacity factor or CF (as defined in Eq. (8)) is used to represent the farm output (to be maximized). Therefore, the WFLO problem is formulated as

$$\begin{aligned}&\max CF(V)\\&V=\{x_1,x_2,\cdots,x_{N_s},y_1,y_2,\cdots,y_{N_s}\}\\ \text{subject to}\quad&\\&g(V)\leq 0\end{aligned} \tag{17}$$

where N_s is the number of turbines for the *sth* combination of sample input parameters; $CF(V)$ is the CF computed using the power generation model in the UWFLO framework [3]; V is the design vector, which denotes the location of turbines; and $g(V)$ defines the minimum inter-turbine spacing constraint ($2D$), as given by

$$\begin{aligned}&g(V)=\textstyle\sum_{\forall i\neq j}\max\{2D-d_{ij},0\}\\ \text{where}\quad&\\&d_{ij}=\sqrt{(x_i-x_j)^2+(y_i-y_j)^2}\\&i,j=1,2,\ldots,N_s\end{aligned} \tag{18}$$

Figures 10(*a*)–10(*d*) illustrate the sensitivity of maximized wind farm CF to all the five input parameters, when the variation of incoming wind speed is located in region I. Similar to case 1 in numerical experiment I, the impact of incoming wind speed is again the dominant factor influencing the maximized wind farm output, irrespective of the choice of wake models.

A completely different scenario evolves when the variation of incoming wind speed restricted to that in region II (case 2). The corresponding results are shown in Figs. 11(*a*)–11(*d*). It is observed (from Fig. 11) that the choice of wake models has a significantly smaller impact on the relative influence of each input parameter compared to that observed for an array layout (Fig. 8). For the array layout, the order of influence of the different input parameters varies across the different wake models. In contrast, for the optimized layout, the order of influence of the different input parameters remains consistent across all four wake models. For example, Figs. 11(*a*)–11(*d*) show that wind speed and nameplate capacity are the strongest and the second strongest influencing factors across all four wake models and land aspect ratio and land area per MW installed have a relatively similar degree of influence on the CF of the optimized wind farm, irrespective of the choice of wake models.

In addition, large values of the total-order indices of all the input parameters are observed. This observation potential again indicates that the input factors are strongly coupled in their

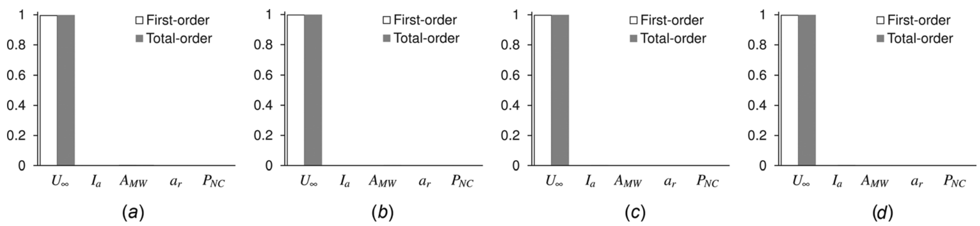

Fig. 10 SA on the maximized wind farm CF with optimized layouts (case 1). (*a*) Jensen model, (*b*) Frandsen model, (*c*) Larsen model, and (*d*) Ishihara model. U_∞: Incoming wind speed; I_a: ambient turbulence; A_{MW}: land area per MW installed; a_r: land aspect ratio; P_{NC}: nameplate capacity.

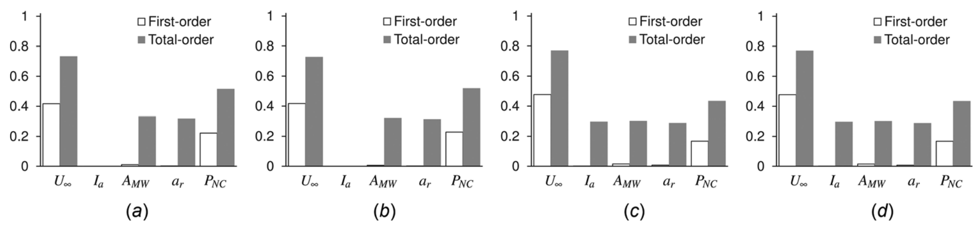

Fig. 11 SA on the maximized wind farm CF with optimized layouts (case 2). (*a*) Jensen model, (*b*) Frandsen model, (*c*) Larsen model, and (*d*) Ishihara model. U_∞: Incoming wind speed; I_a: ambient turbulence; A_{MW}: land area per MW installed; a_r: land aspect ratio; P_{NC}: nameplate capacity.

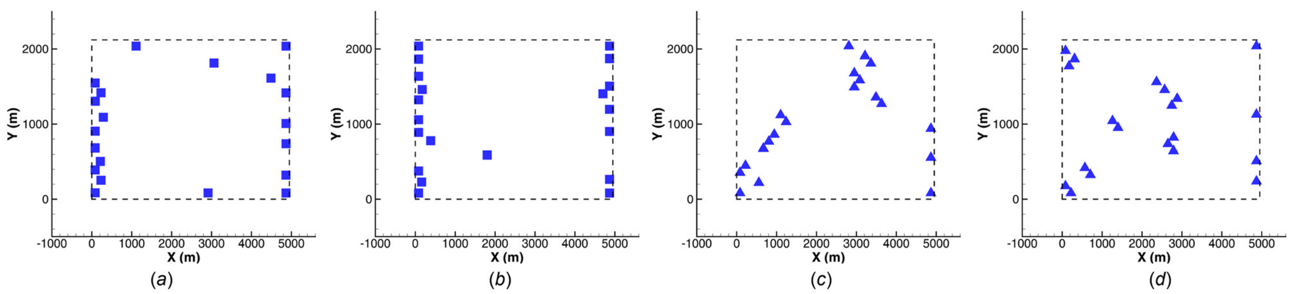

Fig. 12 Illustration of optimized layouts using different wake models. (*a*) Jensen model (CF = 54.34%), (*b*) Frandsen model (CF = 54.00%), (*c*) Larsen model (CF = 54.15%), and (*d*) Ishihara model (CF = 54.69%).

influence on the maximized wind farm CF. It also illustrates that the number of turbines, which is often fixed in conventional WFLO, has a significant impact on the maximized farm output potential, compared to other design factors; especially when the incoming wind speed is close to the turbine rated speed.

Figs. 12(*a*)–12(*d*) illustrate the optimized layouts resulting from the use of the four different wake models; the corresponding maximized values of CF is reported in the figure captions. Input parameters used to generate these layouts are (i) $U = 7.5\,\mathrm{m}\cdot\mathrm{s}^{-1}$, (ii) $I_a = 10\%$, (iii) $A_{\mathrm{MW}} = 35\mathrm{ha/MW}$, (iv) $a_r = 7/3$, and (v) $P_{\mathrm{NC}} = 30\,\mathrm{MW}$ (20 turbines). It is interesting to note that, when using the Jensen or Frandsen wake model in UWFLO, most of the optimally located turbines lie on the left (upstream) and right (downstream) edges of the farm, with very few turbines on the inside of the farm site; in contrast, when using the Larsen or Ishihara wake model, optimally located turbines are placed both inside and on the edges of the wind farm site. This deviation in the optimal turbine arrangement pattern can be in part attributed to the following characteristics of the wake models: In the Larsen or Ishihara wake model, the velocity deficit is a decreasing function of both the downstream from the turbine and the radial distance from the turbine rotor center-line, unlike the Jenson and Frandsen model, where the velocity deficit is only related to the downstream distance from the turbine. Therefore, under the Larsen or Ishihara wake model, there is expected to be a greater tendency to mitigate wake losses by a staggered layout configuration (greater radial separation between upstream and downstream turbines); whereas, under Jenson and Frandsen model, streamwise spacing will likely dominate the effort to mitigate wake losses.

5 Conclusion

In this paper, we explored the sensitivity of wind farm power output to five key natural and design factors, using the e-FAST method. Important findings of this research are summarized below:

(1) When the incoming wind speed is lower than the turbine rated speed, the grossly dominant impact of wind speed on the wind farm power generation is not affected by the choice of wake models.
(2) When the incoming wind speed is allowed to vary in a relatively smaller range, the relative impact of other input factors become more readily evident, and the following observations were made:
   (a) For array-like wind farms, the relative importance of each input parameter varies with the choice of wake models, and significant differences in the sensitivity indices are observed across different wake models. The maximum difference can be up to 70%; where the first-order index of

the incoming wind speed reached approximately 90% for the Frandsen model and only 19% for the Ishihara model.
   (b) For wind farms with optimized layouts, the relative importance of each input parameter is less sensitive to the choice of wake models, i.e., layout optimization has a smoothing effect in this context.
   (c) All input parameters show a high value of the total-order sensitivity indices, which implies that the farm output is strongly sensitive to the coupled impact of these key factors. Hence, assuming fixed values of certain factors during WFLO, e.g., ambient turbulence or land area, will limit the feasibility of the optimal layouts obtained (which is typical of conventional WFLO methods).
(3) The incoming wind speed expectedly drives most of the variance in the wind farm CF, while the nameplate capacity is the most decisive input among all the design factors (influencing the efficiency of optimized wind farm configurations).

This paper has ventured into a scarcely-trodden (but critical) area of understanding the impact of natural/design factors on wind farm performance, by specifically investigating the SA of wind farms with optimized layouts. The upper bound of nameplate capacity was limited to 150 MW in this study due to the high computational expense of SA. Future work should implement more computationally efficient approaches (e.g., using parallel computing or metamodels) to analyze the sensitivity of wind farms with GW size installed capacity. Since different wake models make different assumptions, thereby limiting their applicability to distinct scenarios; a straightforward comparison (as performed here) thus may not yield comprehensive insight into their suitability for WFLO. Future work should therefore also explore more complex SA processes where each model is applied only within its practical feasibility zone defined by its assumptions.

Acknowledgment

Support from the National Science Foundation Award Nos. CMMI-1100948 and CMMI-1437746 is gratefully acknowledged. Any opinions, findings, conclusions, or recommendations expressed in this paper are those of the authors and do not necessarily reflect the views of the NSF.

References

[1] European Wind Energy Association (EWEA), 2009, "*Wind Energy – The Facts: A Guide to the Technology, Economics and Future of Wind Power*," Vol. I, Earthscan, Sterling, VA.
[2] Méchali, M., Barthelmie, R., Frandsen, S., Jensen, L., and Réthoré, P.-E., 2006, "Wake Effects at Horns Rev and Their Influence on Energy Production," Proceedings of the European Wind Energy Conference and Exhibition.
[3] Chowdhury, S., Zhang, J., Messac, A., and Castillo, L., 2013, "Optimizing the Arrangement and the Selection of Turbines for Wind Farms Subject to Varying Wind Conditions," Renewable Energy, **52**, pp. 273–282.
[4] Kusiak, A., Zhang, Z., and Li, M., 2010, "Optimization of Wind Turbine Performance With Data-Driven Models," IEEE Trans. Sustainable Energy, **1**(2), pp. 66–76.
[5] González, J. S., Rodriguez, A. G. G., Mora, J. C., Santos, J. R., and Payan, M. B., 2010, "Optimization of Wind Farm Turbines Layout Using an Evolutive Algorithm," Renewable Energy, **35**(8), pp. 1671–1681.
[6] Du Pont, B. L., and Cagan, J., 2012, "An Extended Pattern Search Approach to Wind Farm Layout Optimization," ASME J. Mech. Des., **134**(8), p. 081002.
[7] Chen, L., and MacDonald, E., 2012, "Considering Landowner Participation in Wind Farm Layout Optimization," ASME J. Mech. Des., **134**(8), p. 084506.
[8] Jensen, N. O., 1983, "A Note on Wind Generator Interaction," Technical Report No. Risø-M-2411, Risø National Laboratory, Roskilde, Denmark.
[9] Katic, I., Højstrup, J., and Jensen, N. O., 1986, "A Simple Model for Cluster Efficiency," Proceedings of the European Wind Energy Conference and Exhibition, Vol. 1, pp. 407–410.
[10] Frandsen, S., Barthelmie, R., Pryor, S., Rathmann, O., Larsen, S., Højstrup, J., and Thøgersen, M., 2006, "Analytical Modelling of Wind Speed Deficit in Large Offshore Wind Farms," Wind Energy, **9**(2), pp. 39–53.
[11] Larsen, G. C., 1988, "A Simple Wake Calculation Procedure," Technical Report No. Risø-M-2760, Risø National Laboratory, Roskilde, Denmark.
[12] Dekker, J. W. M., and Pierik, J. T. G., eds., 1999, *European Wind Turbine Standards II*. ECN Solar & Wind Energy, Petten, The Netherlands.
[13] Ishihara, T., Yamaguchi, A., and Fujino, Y., 2004, "Development of a New Wake Model Based on a Wind Tunnel Experiment," see http://windeng.t.u-tokyo.ac.jp/ishihara/posters/2004_gwp_poster.pdf (last accessed Jan. 2015).
[14] Saltelli, A., Chan, K., and Scott, E. M., 2009, *Sensitivity Analysis (Probability and Statistics)*, Wiley, NY, USA.
[15] Saltelli, A., Tarantola, S., Campolongo, F., and Ratto, M., 2004, *Sensitivity Analysis in Practice: A Guide to Assessing Scientific Models* (Probability and Statistics), Wiley, NY, USA.
[16] Lackner, M. A., Rogers, A. L., and Manwell, J. F., 2008, "Uncertainty Analysis in MCP-Based Wind Resource Assessment and Energy Production Estimation," ASME J. Sol. Energy Eng., **130**(3), p. 031006.
[17] Rocklin, M. D., and Constantinescu, E. M., 2009, "Adjoint Sensitivity Analysis for Wind Power Generation," see www.mcs.anl.gov/papers/P1704.pdf (last accessed Jan. 2015).
[18] Kubik, M. L., Coker, P. J., and Hunt, C., 2011, "Using Meteorological Wind Data to Estimate Turbine Generation Output: A Sensitivity Analysis," Proceedings of the World Renewable Energy Congress (WREC), pp. 4074–4081.
[19] Capps, S., Hall, A., and Hughes, M., 2012, "Sensitivity of Southern California Wind Energy to Turbine Characteristics," Wind Energy, **17**(1), pp. 141–159.
[20] Fuglsang, P., and Thomsen, K., 1998, "Cost Optimization of Wind Turbines for Large-Scale Off-Shore Wind Farms," Technical Report No. Risø-R-1000, Risø National Laboratory, Roskilde, Denmark.
[21] Haughton, J., Giuffre, D., Barrett, J., and Tuerck, D. G., 2004, "An Economic Analysis of a Wind Farm in Nantucket Sound," see http://www.beaconhill.org/BHIStudies/Windmills2004/WindFarmArmyCorps.pdf.
[22] Dykes, K., Ning, A., Graf, P., Scott, G., Damiani, R., Hand, M., Meadows, R., Musial, W., Moriarty, P., and Veers, P., 2012, "Sensitivity Analysis of Offshore Wind Cost of Energy," Technical Report No. NREL/PO-5000-56411, National Renewable Energy Laboratory, Golden, CO.
[23] Dinwoodie, I., and McMillan, D., 2012, "Sensitivity of Offshore Wind Turbine Operation & Maintenance Costs to Operational Parameters," Proceedings of the 42nd ESReDA Seminar on Risk and Reliability for Wind Energy and other Renewable Sources.
[24] Martínez, E., Jiménez, E., Blanco, J., and Sanz, F., 2010, "LCA Sensitivity Analysis of a Multi-Megawatt Wind Turbine," Appl. Energy, **87**(7), pp. 2293–2303.
[25] Gu, Y., Xie, L., Rollow, B., and Hesselbaek, B., 2011, "Congestion-Induced Wind Curtailment: Sensitivity Analysis and Case Studies," Proceedings of the North American Power Symposium, IEEE.
[26] Zack, J., Natenberg, E., Young, S., Manobianco, J., and Kamath, C., 2010, "Application of Ensemble Sensitivity Analysis to Observation Targeting for Short-Term Wind Speed Forecasting," Technical Report No. LLNL-TR-458086, Lawrence Livermore National Laboratory, Livermore, CA.
[27] Osborn, J., Wood, F., Richey, C., Sanders, S., Short, W., and Koomey, J., 2001, "A Sensitivity Analysis of the Treatment of Wind Energy in the AEO99 Version of NEMS," Technical Report No. LBNL-44070/TP-28529, Lawrence Livermore National Laboratory/National Renewable Energy Laboratory, Berkeley, CA/Golden, CO.
[28] Steinbuch, M., de Boer, W., Bosgra, O., Peters, S., and Ploeg, J., 1988, "Optimal Control of Wind Power Plants," J. Wind Eng. Ind. Aerodyn., **27**(1–3), pp. 237–246.
[29] Johnson, K. E., and Thomas, N., 2009, "Wind Farm Control: Addressing the Aerodynamic Interaction Among Wind Turbines," Proceedings of the American Control Conference (ACC).
[30] Brand, M. S. A. J., and Wisniewski, R., 2011, "A Wind Farm Controller for Load and Power Optimization in a Farm," Proceedings of the IEEE International Symposium on Computer-Aided Control System Design (CACSD).
[31] Kusiak, A., and Song, Z., 2010, "Design of Wind Farm Layout for Maximum Wind Energy Capture," Renewable Energy, **35**, pp. 685–694.
[32] Marden, J. R., Ruben, S. D., and Pao, L. Y., 2013, "A Model-Free Approach to Wind Farm Control Using Game Theoretic Methods," IEEE Trans. Control Syst. Technol., **21**(4), pp. 1207–1214.
[33] GE Energy, 2009, "GE 1.5MW Wind Turbine Series," see http://geosci.uchicago.edu/~moyer/GEOS24705/Readings/GEA14954C15-MW-Broch.pdf (last accessed Jan 2015).
[34] Hansen, M. O. L., 2008, *Aerodynamics of Wind Turbines*, 2nd ed., Earthscan, Sterling, VA.
[35] Sørensen, J. N., and Myken, A., 1992, "Unsteady Actuator Disc Model for Horizontal Axis Wind Turbines," J. Wind Eng. Ind. Aerodyn., **39**(1–3), pp. 139–149.
[36] Larsen, G. C., Madsen, H. A., Bingöl, F., Mann, J., Ott, S., Sørensen, J. N., Okulov, V., Troldborg, N., Nielsen, M., Thomsen, K., Larsen, T. J., and Mikkelsen, R., 2007, "Dynamic Wake Meandering Modeling," Technical Report No. Risø-R-1607, Risø National Laboratory, Roskilde, Denmark.
[37] Churchfield, M., and Lee, S., 2012, "High-fidelity analysis of wind plant and wind turbine fluid physics and structural response using computational fluid dynamics (CFD) and FAST," See wind.nrel.gov/designcodes/simulators/SOWFA/ (last accessed Jan. 2015).
[38] Fleming, P., Gebraad, P., Churchfield, M., Lee, S., Johnson, K., Michalakes, J., and van Wingerden, J.-W., 2013, "Sowfa + Super Controller User's Manual," National Renewable Energy Laboratory, Golden, CO.
[39] Annoni, J., Seiler, P., Johnson, K., Fleming, P., and Gebraad, P., 2014, "Evaluating Wake Models for Wind Farm Control," Proceedings of the American Control Conference (ACC).

[40] Gaumond, M., Réthoré, P.-E., Bechmann, A., Ott, S., Larsen, G. C., Pena Diaz, A., and Kurt, K. S., 2012, "Benchmarking of Wind Turbine Wake Models in Large Offshore Windfarms," Proceedings of the Science of Making Torque From Wind.
[41] Beaucage, P., Brower, M., Robinson, N., and Alonge, C., 2012, "Overview of Six Commercial and Research Wake Models for Large Offshore Wind Farms," Proceedings of the European Wind Energy Associate (EWEA).
[42] Barthelmie, R., and Pryor, S. C., 2013, "An Overview of Data for Wake Model Evaluation in the Virtual Wakes Laboratory," Appl. Energy, **104**, pp. 838–844.
[43] Herbert-Acero, J. F., Probst, O., Réthoré, P.-E., Larsen, G. C., and Castillo-Villar, K. K., 2014, "A Review of Methodological Approaches for the Design and Optimization of Wind Farms," Energies, **7**(11), pp. 6930–7016.
[44] Garza, J., Blatt, A., Gandoin, R., and Hui, S., 2011, "Evaluation of Two Novel Wake Models in Offshore Wind Farms," Proceedings of the European Wind Energy Associate Offshore Conference.
[45] Ott, S., Berg, J., and Nielsen, M., 2011, "Linearised CFD Models for Wakes," Technical Report No. Risø-R-1772, Risø National Laboratory, Roskilde, Denmark.
[46] Chowdhury, S., Zhang, J., Messac, A., and Castillo, L., 2012, "Characterizing the Influence of Land Area and Nameplate Capacity on the Optimal Wind Farm Performance," Proceedings of the 6th ASME International Conference on Energy Sustainability, pp. 1349–1359.
[47] Denholm, P., Hand, M., Jackson, M., and Ong, S., 2009, "Land-Use Requirements of Modern Wind Power Plants in the United States," Technical Report No. NREL/TP-6A2-45834, National Renewable Energy Laboratory, Golden, CO.
[48] Chowdhury, S., Tong, W., Messac, A., and Zhang, J., 2013, "A Mixed-Discrete Particle Swarm Optimization Algorithm With Explicit Diversity-Preservation," Struct. Multidisc. Optim., **47**(3), pp. 367–388.
[49] Saltelli, A., and Bolado, R., 1998, "An Alternative Way to Compute Fourier Amplitude Sensitivity Test (FAST)," Comput. Stat. Data Anal., **26**(4), pp. 445–460.
[50] Cukier, R. I., Fortuin, C. M., Shuler, K. E., Petschek, A. G., and Schaibly, J. H., 1973, "Study of the Sensitivity of Coupled Reaction Systems to Uncertainties in Rate Coefficients. I Theory," J. Chem. Phys., **59**(8), pp. 3873–3878.
[51] Schaibly, J. H., and Shuler, K. E., 1973, "Study of the Sensitivity of Coupled Reaction Systems to Uncertainties in Rate Coefficients. II. Applications," J. Chem. Phys., **59**(8), pp. 3879–3888.
[52] Cukier, R. I., Levine, H. B., and Shuler, K. E., 1975, "Study of the Sensitivity of Coupled Reaction Systems to Uncertainties in Rate Coefficients. III. Analysis of the Approximations," J. Chem. Phys., **63**(3), pp. 1140–1149.
[53] Cukier, R. I., 1978, "Nonlinear Sensitivity Analysis of Multiparameter Model Systems," J. Comput. Phys., **26**(1), pp. 1–42.
[54] IEC-61400-1, 2005, *Wind Turbines—Part 1: Design Requirements*, 3rd ed., International Electrotechnical Commission, Geneva, Switzerland.